CSIRO PUBLISHING

www.publish.csiro.au/journals/ajc

Aust. J. Chem. **2009**, *62*, 711–719

Solid-State and Solution-Phase Conformations of Pseudoproline-Containing Dipeptides

Jack K. Clegg,[A] *James R. Cochrane,*[A] *Nima Sayyadi,*[A] *Danielle Skropeta,*[A] *Peter Turner,*[A] *and Katrina A. Jolliffe*[A,B]

[A]School of Chemistry, The University of Sydney, NSW 2006, Australia.
[B]Corresponding author. Email: jolliffe@chem.usyd.edu.au

The conformations of 14 threonine-derived pseudoproline-containing dipeptides (including four D-*allo*-Thr derivatives) have been investigated by NMR. In solution, the major conformer observed for all dipeptides is that in which the amide bond between the pseudoproline and the preceding amino acid is *cis*. For dipeptides in which the *N*-terminus is protected, the ratio of *cis*- to *trans*-conformers does not depend significantly on the side chain of the *N*-terminal amino acid, or the stereochemistry of the Thr residue. However, for dipeptides bearing a free *N*-terminus, there are significant differences in the ratios of *cis*- to *trans*-conformers depending on the side chain present. Three dipeptides were crystallized and their X-ray structures determined. In two cases, (benzyloxycarbonyl (Cbz)-Val-Thr($\Psi^{Me,Me}$pro)-OMe and Cbz-Val-Thr($\Psi^{Me,Me}$pro)-OH), the dipeptides adopt a *trans*-conformation in the solid state, in contrast to the structures observed in solution. In the third case, (9-fluorenylmethoxycarbonyl (Fmoc)-Val-D-*allo*-Thr($\Psi^{Me,Me}$pro)-OH), a *cis*-amide geometry is observed. These structural differences are attributed to crystal-packing interactions.

Manuscript received: 14 March 2009.
Final version: 5 June 2009.

Introduction

Pseudoprolines ($\Psi^{R,R'}$pro) are oxazolidine or thiazolidine derivatives of serine, threonine, and cysteine residues that form on cyclocondensation of the amino acid with an aldehyde or ketone (Fig. 1). Their five-membered ring structure is reminiscent of a proline residue. These modified amino acid residues were introduced by Mutter and coworkers as temporary protecting groups for peptide synthesis and were found to exert a pronounced effect on the peptide backbone conformation.[1,2] The oxazolidine derivatives are now extensively used as tools to impart better solubility to a growing peptide chain in solid-phase synthesis because they prevent aggregation of growing peptide chains[3,4] and have been found to significantly increase the yields of difficult peptide sequences[5–9] by improving solvation and peptide coupling kinetics. This is attributed to a conformational preference for *cis*-amide bond formation. The ability of $\Psi^{R,R'}$pro residues to induce *cis*-amide bonds is well established by experimental[4,10,11] and theoretical[12] studies. In particular, disubstitution at the 2-C position (e.g. $\Psi^{Me,Me}$pro) strongly favours the *cis*-conformer and can be used to tailor peptide backbone conformation for specific applications. We have recently exploited this conformational ability to improve the head-to-tail cyclization yields of short peptide sequences by incorporation of $\Psi^{Me,Me}$pro residues in the linear precursors.[13,14] We have found that, in some cases, cyclization yields vary substantially depending on the side chain of the amino acids preceding the $\Psi^{Me,Me}$pro residues, suggesting that these may influence the *cis–trans* isomerization of the amide bond.[15] This prompted us to investigate the ratios of *cis*- and *trans*-conformers of several model dipeptides with and without *N*- and *C*-termini protecting groups present, to examine the influence of both side chain and protecting groups on the pseudoproline conformation. Previous studies on the conformations of similar dipeptides have focussed on examining the effects of changing the nature of the $\Psi^{R,R'}$pro derivative (whether it is derived from Ser, Thr, and Cys and changing the 2-C substituents R and R′),[10] but the influence of protecting groups and side chain bulk has not been investigated and is of significance in applying the results obtained from model studies to the conformations of longer peptides. We report here the results of an investigation of the solution-phase *cis*:*trans* ratios of several Xaa-Thr($\Psi^{Me,Me}$pro) derivatives, varying both the Xaa substituents and the protecting groups (or lack thereof) at both *N*- and *C*-termini and including several novel

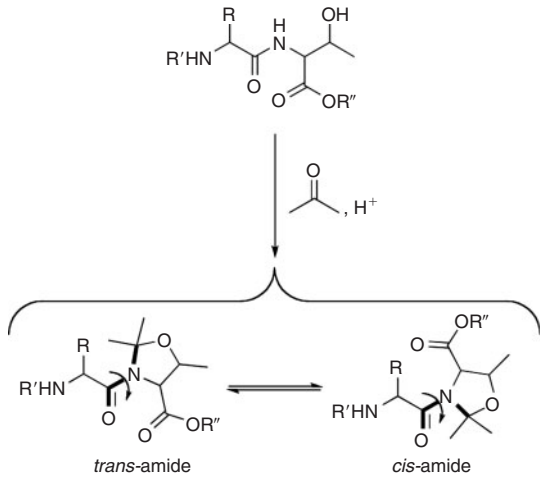

Fig. 1. Synthesis of an Xaa-Thr($\Psi^{Me,Me}$pro) dipeptide and the two conformers accessible by rotation about the Xaa-Thr amide bond.

 10.1071/CH09151 0004-9425/09/070711

D-*allo*-Thr($\Psi^{Me,Me}$pro) derivatives, and their comparison with solid-state structures for three of the compounds as determined by X-ray crystallography.

Results and Discussion

In order to investigate the *cis–trans* isomerization of the peptide bond in differently protected $\Psi^{Me,Me}$pro-containing dipeptides, we prepared several derivatives **1**–**14** (Fig. 2) with either full protection (both *N*- and *C*-termini), *N*-terminus protection or uncapped *N*- and *C*-termini. We positioned Val, Phe, and Gly in the Xaa position to examine the effect the Xaa side chain had on the *cis*:*trans* ratio of the Xaa-Thr($\Psi^{Me,Me}$pro) amide bond. We included four D-*allo*-threonine derivatives (**5**, **6**, **9**, and **12**) because, while the influence of inverting the relative stereochemistry at the α-position of the residue preceding a Thr($\Psi^{Me,Me}$pro) has been reported,[4] the effect of changing the relative stereochemistry between the α- and β-positions on Thr($\Psi^{Me,Me}$pro) formation and conformation has not been previously investigated.

1 R = $CH(CH_3)_2$, R′ = Cbz, R″ = Me
2 R = CH_2Ph, R′ = Cbz, R″ = Me
3 R = H, R′ = Cbz, R″ = Me
4 R = CH_2Ph, R′ = Fmoc, R″ = CH_2CCl_3
7 R = $CH(CH_3)_2$, R′ = Cbz, R″ = H
8 R = CH_2Ph, R′ = Cbz, R″ = H
10 R = $CH(CH_3)_2$, R′ = Fmoc, R″ = H
11 R = CH_2Ph, R′ = Fmoc, R″ = H
13 R = $CH(CH_3)_2$, R′ = R″ = H
14 R = CH_2Ph, R′ = R″ = H

5 R = Cbz, R′ = Me
6 R = Fmoc, R′ = Bn
9 R = Cbz, R′ = H
12 R = Fmoc, R′ = H

Fig. 2. Structures of the Xaa-Thr($\Psi^{Me,Me}$pro) dipeptides.

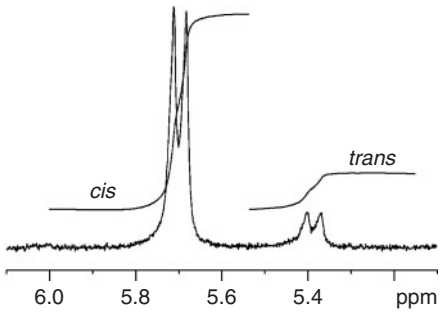

Fig. 3. Portion of the 300 MHz ^{1}H NMR spectrum of **4** illustrating the peaks observed for the carbamate NH of the *cis*- and *trans*-conformers (*cis*:*trans* = 85:15).

Our standard conditions for the synthesis of Xaa-Thr($\Psi^{Me,Me}$pro) derivatives involve treatment of the Thr-containing dipeptides with 2-methoxypropene at 0°C in the presence of an acid catalyst.[13,14] Compounds **1**–**4** were readily synthesized from the corresponding fully protected dipeptides according to this general method. In the case of the D-*allo*-Thr derivatives **5** and **6**, this method gave only low yields of the corresponding pseudoprolines, but these were substantially improved using more forcing conditions (2,2-dimethoxypropane, pyridinium *p*-toluenesulfonate (PPTS), toluene, 80°C). Hydrolysis of the methyl esters of **1**, **2**, and **5**, and hydrogenolysis of the benzyl ester of **6** were performed under standard conditions[13,14] to yield the carboxylic acids **7**–**9** and **12**, respectively. Hydrogenolysis of the benzyloxycarbonyl (Cbz)-groups of **7** and **8** was performed under standard conditions[13] to give **13** and **14**, respectively, Compounds **10** and **11** were prepared according to the method of Mutter et al.[3]

We determined the *cis*:*trans* ratios of the amide bonds in dipeptides **1**–**14** using NMR spectroscopic techniques. In the fully protected dipeptides **1**–**4**, a major and minor set of resonances were clearly observed in both the ^{1}H and ^{13}C NMR spectra, indicating the presence of two conformers in slow exchange (Fig. 3). In all cases, the major conformer was determined to be that with a *cis*-amide bond by the presence of typical nuclear Overhauser effect (NOE) cross peaks observed by 2D NMR rotating frame Overhauser effect spectroscopy (ROESY) and nuclear Overhauser effect correlation spectroscopy (NOESY) experiments (i.e. αH_{i-1}–αH_i and αH_{i-1}–βH_i crosspeaks) that reflect the spatial proximity of the αH_{i-1} and αH_i protons in the *cis*-form.[16] The *cis*:*trans* ratios are given in Table 1. NMR spectra of a representative dipeptide **1** were obtained in a variety of

Table 1. Ratios of *cis*:*trans* conformers as determined by ^{1}H NMR

Dipeptide	Compound no.	Solvent	*cis*:*trans* ratio
CbzNH-Val-$\Psi^{Me,Me}$Thr-OMe	**1**	CD_3CN	85:15
CbzNH-Val-$\Psi^{Me,Me}$Thr-OMe	**1**	[D_6]DMSO	85:15
CbzNH-Val-$\Psi^{Me,Me}$Thr-OMe	**1**	$CDCl_3$	85:15
CbzNH-Val-$\Psi^{Me,Me}$Thr-OMe	**1**	[D_8]toluene	85:15
CbzNH-Val-$\Psi^{Me,Me}$Thr-OMe	**1**	CD_3OD	85:15
CbzNH-Phe-$\Psi^{Me,Me}$Thr-OMe	**2**	CD_3CN	85:15
CbzNH-Gly-$\Psi^{Me,Me}$Thr-OMe	**3**	$CDCl_3$	75:25
FmocNH-Phe-$\Psi^{Me,Me}$Thr-OTce	**4**	CD_3CN	85:15
CbzNH-Val-D-*allo*-$\Psi^{Me,Me}$Thr-OMe	**5**	$CDCl_3$	95:5
FmocNH-Val-D-*allo*-$\Psi^{Me,Me}$Thr-OBn	**6**	$CDCl_3$	90:10
CbzNH-Val-$\Psi^{Me,Me}$Thr-OH	**7**	CD_3CN	80:20
CbzNH-Phe-$\Psi^{Me,Me}$Thr-OH	**8**	CD_3CN	80:20
CbzNH-Val-D-*allo*-$\Psi^{Me,Me}$Thr-OH	**9**	$CDCl_3$	80:20
FmocNH-Val-$\Psi^{Me,Me}$Thr-OH	**10**	CD_3CN	>95:<5
FmocNH-Phe-$\Psi^{Me,Me}$Thr-OH	**11**	CD_3CN	>95:<5
FmocNH-Val-D-*allo*-$\Psi^{Me,Me}$Thr-OH	**12**	CD_3OD	>95:<5
H_2N-Val-$\Psi^{Me,Me}$Thr-OH	**13**	CD_3CN	65:35
H_2N-Phe-$\Psi^{Me,Me}$Thr-OH	**14**	CD_3CN	90:10

solvents (CD_3CN, $CDCl_3$, [D_8]toluene, [D_6]DMSO, CD_3OD) and at varying temperatures (300–370 K in [D_8]toluene) but the ratio of *cis*:*trans* conformers did not change significantly under these conditions. Substitution of the *N*-terminal Val with Phe (**2**) did not affect the ratio of *cis*:*trans* conformers, but a slightly lower proportion of *cis*-amide conformer (75:25) was observed for the Gly-containing dipeptide **3**. This is consistent with the proposal that steric interactions between the methyl groups of the $\Psi^{Me,Me}$Pro and the side chain (or peptide backbone in the case of Gly) of the preceding amino acid are predominantly responsible for the favoured *cis*-conformation of these peptides.[3] Dipeptide **4**, with alternative *N*- and *C*-terminal protecting groups (9-fluorenylmethoxycarbonyl (Fmoc)- and trichloroethyl ester, respectively) had an identical *cis*:*trans* ratio to the Cbz-, methyl ester protected analogue **2**.

For the D-*allo*-Thr derivatives **5** and **6**, a major set of resonances was observed in the ^1H and ^{13}C NMR spectra, with a second set of resonances from a second conformer present but difficult to distinguish owing to their low intensity and signal overlap. The observed major conformers were identified as those having a *cis*-amide bond by the presence of αH_{i-1}–αH_i NOE crosspeaks observed by 2D NMR ROESY and NOESY experiments (Fig. 4). Despite the differences in stereochemistry with the previously discussed systems, an analysis of CPK models indicates that in **5** and **6**, the αH_{i-1} and αH_i protons in the *cis*-conformer are in close proximity, whereas those in the *trans*-conformer are much further away from each other, so an NOE interaction is likely to be observed only for the conformer with a *cis*-amide bond. This proximity in the *cis*-conformer is evident in the X-ray structure of the carboxylic acid derivative **12** (see below).

Removal of the *C*-terminal protecting groups resulted in some changes in the *cis*:*trans* ratios. For the Cbz-protected dipeptides **7**–**9**, a slightly lower amount of the *cis*-conformer was observed than for the analogous methyl esters. More notably, for the dipeptides bearing Fmoc protecting groups, ester hydrolysis resulted in significant increases in the amount of *cis*-conformer present, with only a single (*cis*) conformer observed by ^1H and ^{13}C NMR for **10**, **11** and the D-*allo*-Thr derivative **12**.

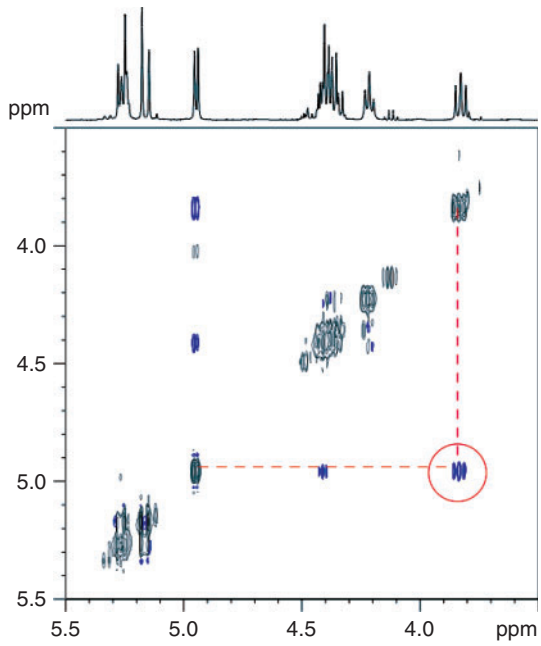

Fig. 4. 400 MHz nuclear Overhauser effect (NOE) correlation spectrum of **6** indicating the NOE interaction between the Val α-H (3.83 ppm) and the D-*allo*-Thr($\Psi^{Me,Me}$pro) α-H (4.95 ppm). Small baseline peaks are attributable to the *trans*-conformer.

In two cases, the effect of deprotection of the *N*-terminus on dipeptide conformation was also investigated. Fully deprotected dipeptides **13** and **14** had significantly different ratios of *cis*:*trans* conformers in comparison with the fully protected analogues **1** and **2**. In contrast to the results observed for the fully protected analogues and *N*-protected peptides where the side chain of the Xaa amino acid had little effect on the ratio of amide bond conformers, for the fully deprotected dipeptides, the *cis*:*trans* ratio depends significantly on the side chain of the *N*-terminal amino acid, with the Val derivative **13** having a significantly lower proportion of the *cis*-conformer than the Phe derivative **14**. This difference cannot easily be explained by steric interactions, although the increased proportion of *cis*-conformer in **14**, which has an aromatic side chain, reflects a similar propensity for Xaa-Pro dipeptides that has been attributed to stabilization of the *cis*-confomer as a result of CH–π interactions between the aromatic side chain and the protons at the α-position of the proline ring.[17] A similar interaction between the protons of the Thr($\Psi^{Me,Me}$pro) methyl groups and the aromatic side chain of the Phe residue would provide a similar stabilization and may explain the observed differences between **13** and **14**, although we did not observe any evidence for such an interaction.

In all 14 Xaa-Thr($\Psi^{Me,Me}$pro) dipeptides that we examined by NMR spectroscopy, the *cis*-conformer was predominant, with *cis*:*trans* ratios varying from 65:35 to >95:<5. For dipeptides bearing *N*-protecting groups, this ratio did not significantly depend on the side chain of the Xaa residue or the stereochemistry of the Thr residue. However, it was affected by the presence of protecting groups at the *N*- and *C*-termini, suggesting that studies of longer peptides are required to provide a better understanding of the influence of the side chain on the conformation of Thr($\Psi^{Me,Me}$pro) peptides.

Solid-State Studies

Although several solution-phase studies of ($\Psi^{R,R'}$pro)-containing peptides have been performed, little is known about the conformations of these peptides in the solid state. To the best of our knowledge, only one X-ray structure of a ($\Psi^{Me,Me}$pro)-containing dipeptide has been reported previously, indicating that Fmoc-Ala-Cys($\Psi^{Me,Me}$pro)-OH retains the *cis*-amide conformation in the solid state, although the amide bond is slightly twisted ($\omega_i = -9.7°$).[18] To obtain further information about the conformations of our Xaa-Thr($\Psi^{Me,Me}$pro) dipeptides, we investigated the solid-state structures of three compounds.

Colourless prismatic crystals of **1** suitable for X-ray crystallography were grown by slow diffusion of diethyl ether into a methanolic solution (see Accessory Publication for *ORTEP* plot). The X-ray analysis indicates that in the solid state, the amide bond preceding the Thr($\Psi^{Me,Me}$pro) adopts a *trans*-conformation (Fig. 5). This is in contrast to the NMR experiments, which indicate that in the solution-phase, the *cis*-conformer predominates (*cis*:*trans* 85:15) independently of solvent or temperature. In the solid state, the amide bond (N(1)–C(9)) is 1.3517(13) Å in length, which is similar to the length of the bond between the Val nitrogen atom and the Cbz protecting group (N(2)–C(14) = 1.3474(14) Å). The amide bond is slightly twisted ($\omega_i = 171.36(11)°$), indicating the steric hindrance that

would result between the Thr($\Psi^{Me,Me}$pro) methyl substituents and the Val side chain if it were planar.

An analysis of the crystal packing shows a strong carbamate (N(2)) to Thr($\Psi^{Me,Me}$pro) oxygen (O(1)) hydrogen bond (see Table 2) as the most significant motif present within the lattice. This interaction results in the formation of infinite one-dimensional polymeric chains of molecules that propagate down the crystallographic *b*-axis. A section of one of these chains is shown in Fig. 5. Given the energy difference between the *cis*- and *trans*-conformers of $\Psi^{Me,Me}$pro dipeptides is ~62–75 kJ mol^{-1},[10] the stabilization introduced in the solid state by this hydrogen-bonding interaction may explain the differences observed between the solution-phase and solid-state conformations of this dipeptide.

Colourless plate-like crystals of **7**, the free-acid analogue of **1**, were isolated by slow diffusion of diethyl ether into a methanol solution and subjected to a crystallographic study (see Accessory Publication for *ORTEP* plot). The X-ray analysis revealed that **7** adopts a conformation ($\omega_i = 174.27(17)°$) in the solid state that is almost identical to that of **1** (Fig. 6), again in contrast to the solution-phase conformation of this molecule. In fact, both **1** and **7** crystallize in the same chiral space group (orthorhombic $P2_12_12_1$) with similar unit cells. In both structures, the *a* and *b* axis lengths are comparable, while the *c* axis lengths differ by only 2.1 Å. Given their chemical similarity, their structural similarity is not surprising, but suggests the possibility of use of species such as these in crystal engineering studies. Such a possibility is further demonstrated by the analysis of the crystal packing.

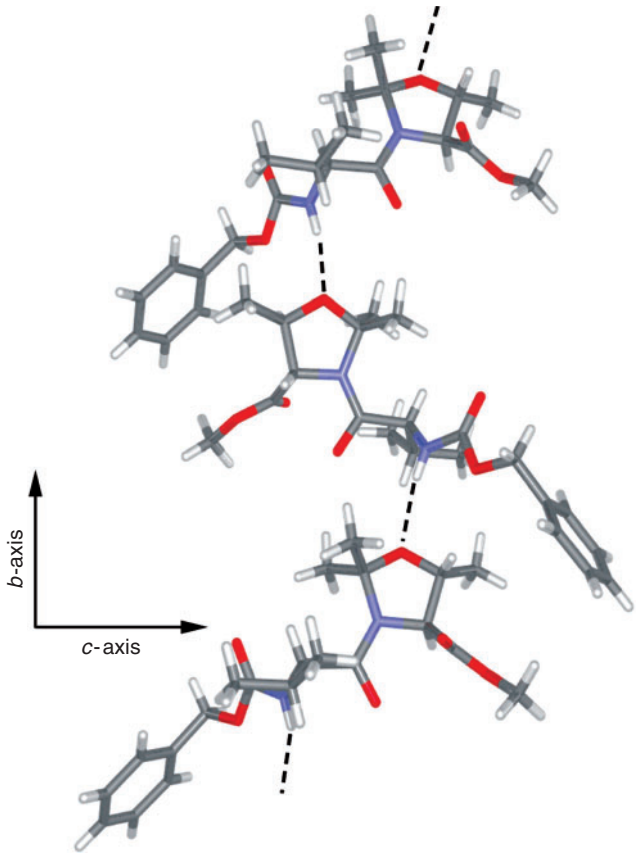

Fig. 5. A schematic representation of the one-dimensional polymeric chain formed in **1**. Dashed lines indicate hydrogen-bonding interactions.

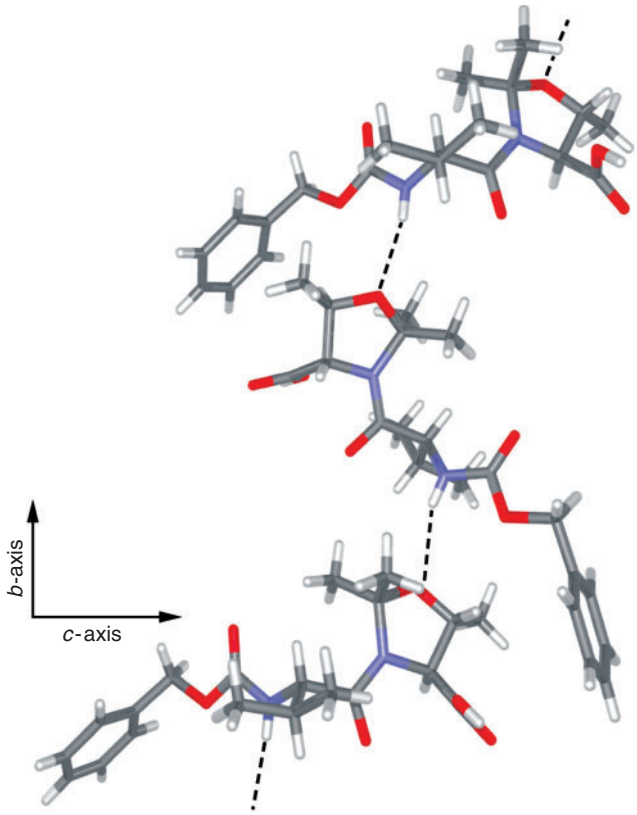

Fig. 6. A schematic representation of the one-dimensional polymeric chain formed in **7** through carbamate–oxygen hydrogen bonds. Dashed lines indicate hydrogen-bonding interactions.

Table 2. Hydrogen bond geometry from X-ray structures of 1, 7 and 12 where D indicates the H-bond donor and A the acceptor

D	H	A	D–H [Å]	H–A [Å]	D–A [Å]	DHA [°]
1						
N(2)	H(2N)	O(1)^{A}	0.850(14)	2.221(15)	3.0534(13)	166.1(13)
7						
H(2O)	H(2O)	O(3)^{B}	0.83(3)	1.87(3)	2.684(2)	164(3)
N(2)	H(2N)	O(1)^{A}	0.82(3)	2.34(3)	3.146(2)	168(2)
12						
N(2)	H(1N)	O(8)^{C}	0.89(5)	1.88(5)	2.760(3)	171(4)
N(4)	H(2N)	O(4)^{C}	0.81(4)	2.32(4)	3.060(3)	152(4)

Symmetry operators: $^{A}-x, y+1/2, -z+1/2$; $^{B}-x+1/2, -y, z+1/2$; $^{C}x-y, -y, -z+2/3$.

Much like **1**, molecules of **7** pack along the crystallographic *b*-axis to form a one-dimensional polymeric chain through carbamate (N(2)) to pseudoproline oxygen (O(1)) hydrogen-bonding interactions (see Table 2). A portion of this chain is shown in Fig. 6.

The presence of the free carboxylic acid group in **7** (compared with **1**) adds an additional site for hydrogen bonding. Although this site does bind to the corresponding carboxylic site in adjacent molecules, unexpectedly, it does not bind in the classic carboxylic acid dimer and instead forms a polymeric chain (see Fig. 7), which propagates along the crystallographic *a*-axis at ~90° to the amide–oxygen hydrogen-bonding chain. Overall, these two sets of hydrogen-bonding interactions combine to form infinite two-dimensional sheet-like arrays that stack parallel to the crystallographic *ab*-plane.

The D-*allo*-Thr derivative **12** also crystallizes in the orthorhombic $P2_12_12_1$ space group. Colourless plate-like crystals were grown by the slow evaporation of a chloroform solution and there are two chloroform solvent molecules present in the lattice for each peptide molecule. In contrast to the previous two structures, in this case the amide bond has the expected *cis* geometry ($\omega_i = -1.7(5)°$). The structure is given in Fig. 8 and illustrates the short distance between the two α-protons (H(2) and H(9)) observed in the NOESY spectrum of this molecule.

Once again, the dominant crystal-packing effects are hydrogen-bonding interactions. However, in contrast to **1** and **7**, these do not involve the Thr($\Psi^{Me,Me}$pro) oxygen. Interestingly, again despite the presence of a carboxylic acid, the dimeric carboxylic acid motif is not present. Instead the carboxylic acid binds to the carbamate (N(2)) nitrogen and amide (O(4)) oxygen of the Val residue (Table 2), forming an infinite one-dimensional polymer (Fig. 9) along the *a*-axis. There is also a weak methyl–π interaction within the lattice. There are several non-classical hydrogen-bonding interactions present in the lattice, with the chloroform solvent molecules acting as H-bond donors and oxygen atoms as acceptors (Fig. 10). In particular, the presence of an H-bond between chloroform and the Thr($\Psi^{Me,Me}$pro) oxygen (O(3)) is notable, as this prevents the formation of the carbamate to Thr($\Psi^{Me,Me}$pro) oxygen H-bonds that are the predominant crystal packing interactions in **1** and **7**. This may explain the conformational differences observed for **12** (*cis*-amide) in comparison with **1** and **7** (*trans*-amide) in the solid state. It is notable that no solvent is present in the crystal lattices of **1** and **7**, despite their crystallization from methanol, a solvent that is more likely to form H-bonds than chloroform.

Conclusions

In solution, the predominant conformer for Xaa-Thr($\Psi^{Me,Me}$pro) dipeptides is that in which the amide bond between the Xaa and Thr($\Psi^{Me,Me}$pro) residues adopts a *cis* geometry. For dipeptides bearing both *N*- and *C*-terminal protecting groups, the ratio of *cis*:*trans* conformers does not depend strongly on solvent, temperature or the size of the Xaa side chain. It is notable that the relative stereochemistry of the Thr($\Psi^{Me,Me}$pro) residue does not have a significant impact on the *cis*:*trans* amide bond ratio, with D-*allo*-Thr-containing peptides having similar (or enhanced) conformational preferences for the *cis*-isomer to the L-Thr derivatives in solution. It has previously been shown that the relative stereochemistry between the Xaa and ($\Psi^{Me,Me}$pro) α-carbons does not have a significant influence on the amide bond conformation.[4] Minor differences in the *cis*:*trans* ratios are observed for *N*-protected dipeptides with a free carboxylic acid, depending on whether the *N*-protecting group is Cbz or Fmoc, with Fmoc-protected dipeptides having a higher proportion (>95%) of *cis*-conformer. However, for dipeptides with free *N*- and *C*-termini, the *cis*:*trans* ratio is strongly influenced by the Xaa side chain, with **14**, which has an aromatic side

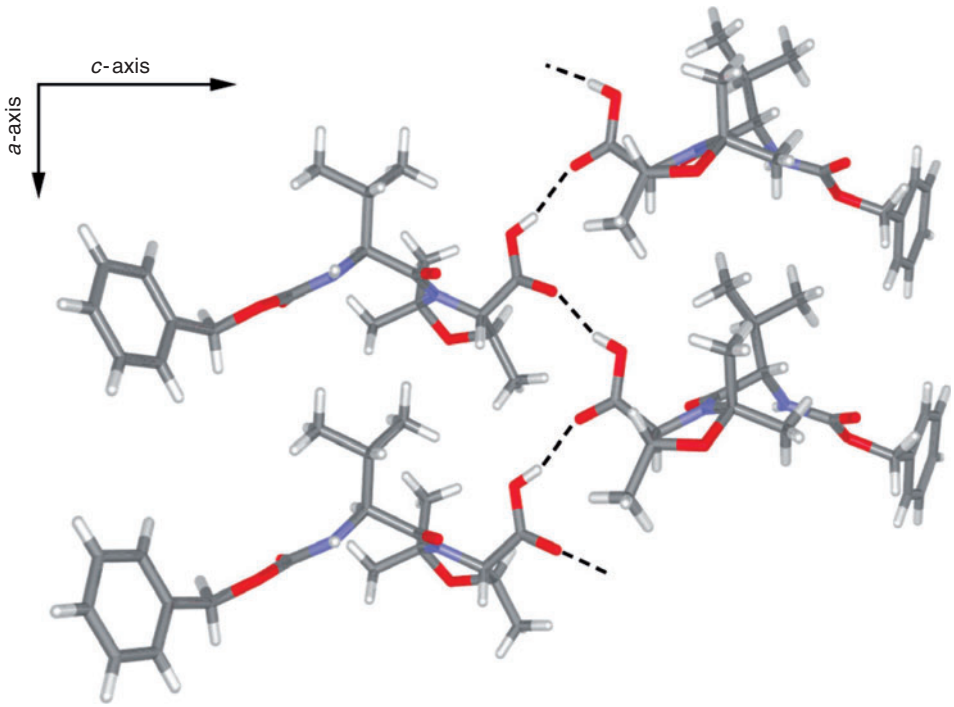

Fig. 7. A schematic representation of the one-dimensional polymeric chain formed via carboxylic acid–carboxylic acid hydrogen bonds in **7**. Dashed lines indicate hydrogen-bonding interactions.

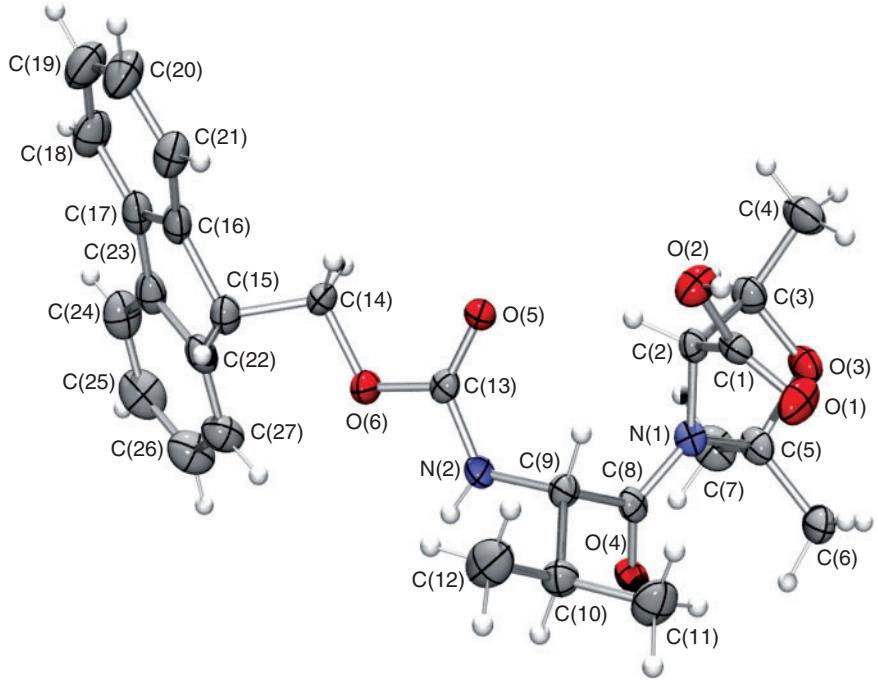

Fig. 8. An *ORTEP* representation of **12** shown with 50% probability ellipsoids. Chloroform solvent molecules omitted for clarity.

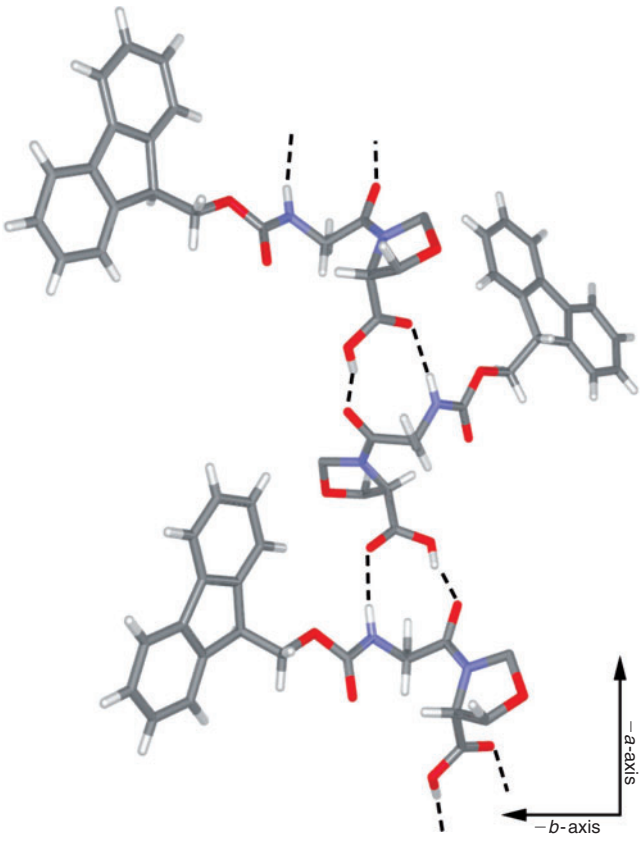

Fig. 9. A schematic representation of the one-dimensional polymeric chain formed in **12**. Dashed lines indicate hydrogen-bonding interactions. Val side chains and Thr($\Psi^{Me,Me}$pro) methyl groups have been removed for clarity.

chain, having a significantly higher proportion of *cis*-conformer than **13**, which bears an isopropyl side chain. This suggests that an analysis of the conformation of longer ($\Psi^{Me,Me}$pro)-containing peptides must be performed on the fully deprotected

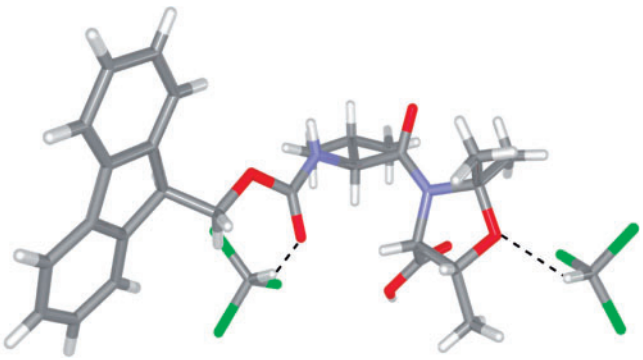

Fig. 10. A schematic representation of **12** illustrating the H-bonding interactions observed with $CHCl_3$ solvent molecules.

systems to avoid any influence of the protecting groups on conformation.

In the solid state, **1** and **7** adopt a *trans*-amide bond conformation, although in both cases the amide bond is slightly twisted. This directly contrasts with their solution structures and can be attributed to crystal-packing effects, with X-ray structures of both **1** and **7** showing a predominant carbamate (N) to Thr($\Psi^{Me,Me}$pro) oxygen hydrogen-bonding interaction in the crystal lattice. The stabilization provided in the solid state by this hydrogen-bonding interaction and other crystal lattice effects is clearly greater than the 62–75 kJ mol^{-1} stabilization of the *cis*-conformer relative to the *trans*-conformer in solution.[10] In contrast, **12** adopts a *cis*-amide bond in both solution and the solid state. In this case, the co-crystallized chloroform solvent molecules act as hydrogen bond donors to the D-*allo*-Thr($\Psi^{Me,Me}$pro) oxygen hydrogen-bond acceptor, preventing the formation of the stabilizing carbamate–pseudoproline oxygen hydrogen bonds observed for **1** and **7**. An investigation

of the solution and solid-state structures of longer $\Psi^{Me,Me}$pro-containing peptides and the relationship between peptide conformation and head-to-tail cyclization yields is ongoing in our laboratories.

Experimental

Synthesis

Preparative column chromatography was carried out using Ajax Finechem silica gel (SiO_2, 0.040–0.063 mm) with the indicated solvents. Melting points were determined using a Gallenkamp melting point apparatus and are reported in degrees Celsius (uncorrected). NMR spectra were recorded on a 200, 300, or 400 MHz spectrometer. The solvent ^1H and ^{13}C signals, δ_H 7.26 for residual $CHCl_3$ and δ_C 77.0 for $CDCl_3$; δ_H 3.31 and δ_C 49.0 for [D_4]MeOH; δ_H 2.50 and δ_C 39.5 for [D_6]DMSO; δ_H 1.94 and δ_C 1.3 for CD_3CN were used as internal references. Signal assignments are based on a combination of 1D (including ^1H selective homonuclear decoupling and ^{13}C Distortionless Enhancement by Polarisation Transfer (DEPT)) and 2D spectral data (including H,H-correlation spectroscopy, heteronuclear multiple bond correlation, heteronuclear single-quantum correlation, and gradient-NOESY (gr-NOESY)). Optical rotations were measured on a dual-wavelength polarimeter in a 0.25-dm cell at 22°C using the indicated spectroscopic grade solvents. Elemental analyses were performed by Campbell Microanalytical Laboratories. Compounds **1**–**4**, and **7**–**8** were synthesized from the appropriately protected dipeptides according to previously reported methods.[13–15] Compounds **10** and **11** were prepared according to the method of Mutter and coworkers.[3] Compounds **13** and **14** were prepared on removal of the Cbz protecting groups from **7** and **8**, respectively, by hydrogenolysis under previously reported conditions[13] and used without purification for ^1H NMR studies.

*Cbz-L-Val-D-*allo-*Thr($\Psi^{Me,Me}$pro)-OMe* **5**

Dimethoxypropane (1.00 mL, 8.14 mmol) and pyridinium-*p*-toluene sulfonate (124 mg, 0.540 mmol) were added to a solution of Cbz-L-Val-D-*allo*-Thr-OMe (0.533 mg, 1.46 mmol) dissolved in toluene (25 mL) and the mixture stirred at 80°C for 16 h. The solution was cooled to ambient temperature and dichloromethane (100 mL) was added. The solution was then washed with saturated aqueous $NaHCO_3$ (100 mL) and the aqueous layer re-extracted with dichloromethane (2 × 30 mL). The combined organic layers were then washed with brine (2 × 100 mL), dried (Na_2SO_4), and the solvent removed under reduced pressure. The crude product was purified by flash chromatography (4:1 v/v dichloromethane/EtOAc). Concentration of the appropriate fractions (R_F 0.74) yielded *title peptide* **5** (474 mg, 80%) as a yellow oil. $[\alpha]_D$ +8.40° (*c* 1.0 in $CHCl_3$). δ_H (200 MHz, $CDCl_3$) 7.33 (5H, m, ArH), 5.09 (1H, d, *J* 9.1, Val(NH)), 5.01 (2H, s, Cbz(CH_2)), 4.98 (1H, d, *J* 6.1, ThrΨ(α-CH)), 4.40 (1H, m, ThrΨ(β-CH)), 3.85 (1H, m, Val(α-CH)), 3.78 (3H, s, Me), 1.91–1.74 (1H, m, Val(β-CH)), 1.68 (3H, s, Me), 1.57 (3H, s, Me), 1.28 (3H, d, *J* 6.3, Thr(γ-CH_3)), 0.93 (3H, d, *J* 6.7, Val(γ-CH_3)), 0.85 (3H, d, *J* 6.7, Val(γ-CH_3)). δ_C (75 MHz, $CDCl_3$) 170.2, 169.9, 156.6, 136.4, 128.5, 128.2, 127.9, 96.4, 72.5, 70.0, 63.6, 57.0, 52.0, 27.9, 24.9, 23.6, 19.7, 18.0, 15.2. *m/z* (electrospray ionization (ESI)) 429 $[M + Na]^+$ (100%), 356 (40), 349 (30); *m/z* (high resolution mass spectroscopy (HRMS) ESI, MNa^+) Calc. for $C_{21}H_{30}N_2O_6{\cdot}Na$ 429.1996; found 429.1990.

*Cbz-L-Val-D-*allo-*Thr($\Psi^{Me,Me}$pro)-OH* **9**

NaOH (400 mg, 0.100 mol) was dissolved in distilled water (2 mL) and added to a solution of **5** (650 mg, 1.60 mmol) in THF (3 mL) and methanol (3 mL). The reaction mixture was stirred for 24 h before the solution was partitioned between 1 M HCl (50 mL) and dichloromethane (50 mL). The aqueous phase was extracted with dichloromethane (2 × 20 mL) and the combined organic phases were washed with brine (2 × 100 mL), then dried (Na_2SO_4). Removal of the solvent under reduced pressure gave the *title compound* **9** (0.390 g, quantitative) as a yellow foam. δ_H (200 MHz, $CDCl_3$) 7.33 (5H, s, ArH), 5.47 (1H, d, *J* 9.3, Val(NH)), 5.10 (2H, s, Cbz(CH_2)), 5.02 (1H, d, *J* 6.1, ThrΨ(α-CH)), 4.47–4.41 (1H, ThrΨ(β-CH)), 3.94–3.65 (1H, m, Val(α-CH)), 2.0–1.96 (1H, m, Val(β-CH)), 1.84 (3H, s, Me), 1.59 (3H, s, Me), 1.37 (3H, d, *J* 6.1, Thr(γ-CH_3)), 0.93 (3H, d, *J* 6.7, Val(γ-CH_3)), 0.87 (3H, d, *J* 6.7, Val(γ-CH_3)). δ_C (75 MHz, $CDCl_3$) 173.1, 170.4, 156.9, 136.3, 128.6, 128.2, 127.8, 96.7, 72.6, 67.1, 63.6, 59.6, 29.5, 24.9, 23.6, 19.6, 18.2, 15.3. *m/z* (ESI) 415.1 $[M + Na]^+$ (100%), 393 (10), 357 (5), 353 (10), 341 (5), 335 (15); *m/z* (HRMS ESI, MNa^+) Calc. for $C_{20}H_{28}N_2O_6{\cdot}Na$ 415.1857; found 415.1857.

*Fmoc-Val-D-*allo-*Thr($\Psi^{Me,Me}$pro)-OBn* **6**

Dimethoxypropane (472 μL, 3.85 mmol) and pyridinium-*p*-toluene sulfonate (60.0 mg, 0.231 mmol) were added to a solution of Fmoc-Val-D-*allo*-Thr-OBn (408 mg, 0.769 mmol) dissolved in toluene (10 mL) and the mixture was heated at reflux for 16 h. The solution was cooled to ambient temperature before diluting with EtOAc (100 mL). The solution was then washed with saturated aqueous $NaHCO_3$ (100 mL), then the aqueous layer was re-extracted with EtOAc (2 × 50 mL). The combined organic layers were then washed with brine (2 × 100 mL), dried (Na_2SO_4), and the solvent removed under reduced pressure. The crude product was purified by flash chromatography (2:1 v/v hexane/EtOAc) to give the *title compound* **6** as a yellow oil (329 mg, 75%). $[\alpha]_D$ +29° (*c* 0.92 in $CHCl_3$). δ_H (400 MHz, $CDCl_3$) 7.76 (2H, d, *J* 7.6, ArH), 7.57, (2H, d, *J* 7.6, ArH), 7.42–7.28 (9H, m, ArH), 5.25 (1H, d, *J* 9.4, Val(NH)), 5.26 (1H, d, *J* 12.3, Cbz(CH_2)), 5.16 (1H, d, *J* 12.3, Cbz(CH_2)), 4.95 (1H, d, *J* 6.0, ThrΨ(α-CH)), 4.37 (3H, m), 4.22 (1H, t, *J* 6.8, Fmoc(CH)), 3.83 (m, 1H, Val(α-CH)), 1.86 (1H, m, Val(β-CH)), 1.74 (3H, s, Me), 1.59 (3H, s, Me), 1.22 (3H, d, *J* 6.7, Thr(γ-CH_3)), 0.83 (3H, d, *J* 6.7, Val(γ-CH_3)), 0.71 (3H, *J* 6.7, Val(γ-CH_3)). δ_C (100 MHz, $CDCl_3$) 169.4, 169.3, 156.4, 143.7, 143.1, 134.9, 128.9, 128.7, 127.7, 125.1, 125.0, 96.3, 72.7, 67.3, 67.0, 63.4, 59.0, 47.1, 30.5, 24.9, 23.6, 19.4, 17.7, 15.2. *m/z* (ESI) 570 $[M + Na]^+$ (100%), 571 (35); *m/z* (HRMS ESI, MNa^+) Calc. for $C_{34}H_{38}N_2O_6{\cdot}Na$ 593.2622; found 593.2614.

*Fmoc-Val-D-*allo-*Thr($\Psi^{Me,Me}$pro)-OH* **12**

Compound **6** (200 mg, 0.350 mmol) was dissolved in 10 mL of dry THF and 10% Pd/C catalyst was added. The reaction flask was purged with H_2 and evacuated three times and the solution was left stirring under an atmosphere of H_2 for 48 h. The solution was then filtered through a pad of Celite and the solvent removed under reduced pressure. The residue was purified by flash chromatography (100:5:1 $CHCl_3$/MeOH/AcOH) to give the desired peptide as a colourless foam. Recrystallization ($CHCl_3$) afforded the *title compound* **12** as colourless needles (138 mg, 82%). Mp 95–98°C. $[\alpha]_D$ +19° (*c* 0.99 in $CHCl_3$). (Found C 67.2, H 6.6, N 5.6. $C_{27}H_{32}N_2O_6$ requires C 67.5, H 6.7, N 5.8%.) δ_H (400 MHz, MeOD) 7.75 (2H, d, *J* 7.9, ArH),

7.58 (2H, d, *J* 7.9, ArH), 7.4–7.3 (4H, m, ArH), 5.05 (1H, d, *J* 6.1, ThrΨ(α-CH)), 4.45 (1H, m, ThrΨ(β-CH)), 4.40 (2H, d, *J* 6.8, Fmoc(CH_2)), 4.24 (1H, t, *J* 6.8, Fmoc(CH)), 3.80 (1H, m, Val(α-CH)), 1.87 (1H, m, Val(β-CH)), 1.77 (3H, s, Me), 1.61 (3H, s, Me), 1.38 (3H, d, *J* 6.0, Thr(γ-CH_3)), 0.94 (3H, d, 6.6, Val(γ-CH_3)), 0.88 (3H, d, *J* 6.6, Val(γ-CH_3)). δ_C (100 MHz, $CDCl_3$) 173.3, 170.0, 156.6, 143.6, 141.3, 127.7, 127.1, 125.1, 120.0, 96.5, 72.4, 67.2, 63.4, 59.4, 47.0, 31.6, 24.8, 23.5, 19.4, 18.1, 15.2. *m/z* (ESI) 503 $[M + Na]^+$ (100%), 504 (30); *m/z* (HRMS EI, MNa^+) Calc. for $C_{27}H_{32}N_2O_6{\cdot}Na$ 503.2158; found 503.2161.

Crystallography

Data for **1**, **7**, and **12** were collected with ω scans to ~56° 2θ using a Bruker SMART 1000 diffractometer employing graphite-monochromated Mo-Kα radiation generated from a sealed tube (0.71073 Å) at 150(2) K. Data integration and reduction were undertaken with *SAINT* and *XPREP*.[19] Subsequent computations were carried out using the *teXsan*, *WinGX-32*, and *XTAL* graphical user interfaces.[20–22]

Structures were solved by direct methods using *SIR97*.[23] Multiscan empirical absorption corrections were applied to the dataset using the program *SADABS*.[24] Gaussian[25] adsorption corrections were applied with *XPREP*.[19] Data were refined and extended with *SHELXL-97*.[26] In general, non-hydrogen atoms with occupancies greater than 0.5 were refined anisotropically. Carbon-bound hydrogen atoms were included in idealized positions and refined using a riding model. Oxygen- and nitrogen-bound hydrogen atoms were first located in the difference Fourier map before refinement. Where these hydrogen atoms could not be located, they were not modelled. Disorder was modelled using standard crystallographic methods including constraints and restraints where necessary. Crystal and structure refinement data, including any specific refinement details are summarized below. Crystallographic information files reported in the present manuscript have been deposited with the Cambridge Crystallographic Data Centre as supplementary publication numbers CCDC 723749–723751. Copies of the data are available free of charge from the CCDC, 12 Union Road, Cambridge, CB2 1EZ, UK (fax: (+44) 1223 336 033; email: deposit@ccdc.cam.ac.uk).

*Crystal Data for **1***

Formula $C_{21}H_{30}N_2O_6$, *M* 406.47, orthorhombic, space group $P2_12_12_1$(#19), *a* 6.894(2), *b* 14.248(2), *c* 21.863(2) Å, *V* 2147.5(7) $Å^3$, D_c 1.257 g cm^3, *Z* 4, crystal size 0.493 by 0.438 by 0.219 mm, colourless, habit prism, temperature 150(2) K, λ(MoKα) 0.71073 Å, μ(MoKα) 0.092 mm^{-1}, $T(\text{Gaussian})_{min,max}$ 0.961, 0.983, $2\theta_{max}$ 56.60, *hkl* range −9 9, −18 19, −29 29, *N* 21262, N_{ind} 5151(R_{merge} 0.0295), N_{obs} 4802($I > 2\sigma(I)$), N_{var} 272, residuals* *R*1(*F*) 0.0301, *wR*2(F^2) 0.0708, GoF(all) 1.088, $\Delta\rho_{min,max}$ −0.212, 0.200 e^- $Å^{-3}$.

*$R1 = \Sigma||F_o| - |F_c||/\Sigma|F_o|$ for $F_o > 2\sigma(F_o)$; $wR2 = [\Sigma w(F_o^2 - F_c^2)^2/\Sigma(wF_c^2)^2]^{1/2}$ all reflections $w = 1/[\sigma^2(F_o^2) + (0.03P)^2 + 0.3P]$ where $P = (F_o^2 + 2F_c^2)/3$.

*Crystal Data for **7***

Formula $C_{20}H_{28}N_2O_6$, *M* 392.44, Orthorhombic, space group $P2_12_12_1$(#19), *a* 6.8768(17), *b* 14.555(4), *c* 19.733(5) Å, *V* 1975.2(9) $Å^3$, D_c 1.320 g cm^{-3}, *Z* 4, crystal size 0.285 by 0.275 by 0.101 mm, colourless, habit plate, temperature 150(2) K, λ(MoKα) 0.71073 Å, μ(MoKα) 0.098 mm^{-1}, $T(\text{Gaussian})_{min,max}$ 0.974, 0.993, $2\theta_{max}$ 56.88, *hkl* range −9 9, −19 19, −26 26, *N* 19587, N_{ind} 4776(R_{merge} 0.0399), N_{obs} 4232($I > 2\sigma(I)$), N_{var} 266, residuals* *R*1(*F*) 0.0356, *wR*2(F^2) 0.0952, GoF(all) 1.132, $\Delta\rho_{min,max}$ −0.232, 0.287 e^- $Å^{-3}$.

*$R1 = \Sigma||F_o| - |F_c||/\Sigma|F_o|$ for $F_o > 2\sigma(F_o)$; $wR2 = [\Sigma w(F_o^2 - F_c^2)^2/\Sigma(wF_c^2)^2]^{1/2}$ all reflections $w = 1/[\sigma^2(F_o^2) + (0.05P)^2 + 0.3P]$ where $P = (F_o^2 + 2F_c^2)/3$.

*Crystal Data for **12***

Formula $C_{29}H_{34}Cl_6N_2O_6$, *M* 719.28, orthorhombic, space group $P2_12_12_1$(#19), *a* 13.335(4), *b* 14.547(4), *c* 17.684(5) Å, *V* 3430.2(16) $Å^3$, D_c 1.393 g cm^{-3}, *Z* 4, crystal size 0.400 by 0.350 by 0.100 mm, colourless, habit plate, temperature 150(2) K, λ(MoKα) 0.71073 Å, μ(MoKα) 0.543 mm^{-1}, $T(SADABS)_{min,max}$ 0.860, 0.947, $2\theta_{max}$ 56.72, *hkl* range −17 17, −19 19, −22 22, *N* 34065, N_{ind} 8220(R_{merge} 0.0614), N_{obs} 5400($I > 2\sigma(I)$), N_{var} 399, residuals* *R*1(*F*) 0.0639, *wR*2(F^2) 0.1454, GoF(all) 1.010, $\Delta\rho_{min,max}$ −0.515, 0.664 e^- $Å^{-3}$.

*$R1 = \Sigma||F_o| - |F_c||/\Sigma|F_o|$ for $F_o > 2\sigma(F_o)$; $wR2 = [\Sigma w(F_o^2 - F_c^2)^2/\Sigma(wF_c^2)^2]^{1/2}$ all reflections $w = 1/[\sigma^2(F_o^2) + (0.0590P)^2 + 2.5336P]$ where $P = (F_o^2 + 2F_c^2)/3$.

Accessory Publication

NOESY NMR spectrum of **12** and *ORTEP* plots of **1** and **7** are available from the Journal's website.

Acknowledgements

We thank the Australian Research Council for financial support and for the award of a Queen Elizabeth II research fellowship to K.A.J.

References

[1] T. Haack, M. Mutter, *Tetrahedron Lett.* **1992**, *33*, 1589. doi:10.1016/S0040-4039(00)91681-2

[2] T. Wöhr, M. Mutter, *Tetrahedron Lett.* **1995**, *36*, 3847. doi:10.1016/0040-4039(95)00667-2

[3] T. Wöhr, F. Wahl, A. Hefzi, B. Rohwedder, T. Sato, X. Sun, M. Mutter, *J. Am. Chem. Soc.* **1996**, *118*, 9218. doi:10.1021/JA961509Q

[4] P. Dumy, M. Keller, D. E. Ryan, B. Rohwedder, T. Wöhr, M. Mutter, *J. Am. Chem. Soc.* **1997**, *119*, 918. doi:10.1021/JA962780A

[5] I. Coin, M. Beyermann, M. Bienert, *Nat. Protocols* **2007**, *2*, 3247. doi:10.1038/NPROT.2007.454

[6] F. García-Martín, P. White, R. Steinauer, S. Cote, J. Tulla-Puche, F. Albericio, *Biopolymers* **2006**, *84*, 566. doi:10.1002/BIP.20564

[7] G.-A. Cremer, H. Tanae, A. F. Delmas, *J. Pept. Sci.* **2006**, *12*, 437. doi:10.1002/PSC.746

[8] A. Abedini, D. P. Raleigh, *Org. Lett.* **2005**, *7*, 693. doi:10.1021/OL047480+

[9] M. Keller, A. D. Miller, *Bioorg. Med. Chem. Lett.* **2001**, *11*, 857. doi:10.1016/S0960-894X(01)00085-3

[10] M. Keller, C. Sager, P. Dumy, M. Schutkowski, G. S. Fischer, M. Mutter, *J. Am. Chem. Soc.* **1998**, *120*, 2714. doi:10.1021/JA973966S

[11] M. Mutter, T. Wöhr, S. Gioria, M. Keller, *Biopolymers* **1999**, *51*, 121. doi:10.1002/(SICI)1097-0282(1999)51:2<121::AID-BIP2>3.0.CO;2-O

[12] Y. Che, G. R. Marshall, *Biopolymers* **2006**, *81*, 392. doi:10.1002/BIP.20431

[13] D. Skropeta, K. A. Jolliffe, P. Turner, *J. Org. Chem.* **2004**, *69*, 8804. doi:10.1021/JO0484732

[14] N. Sayyadi, D. Skropeta, K. A. Jolliffe, *Org. Lett.* **2005**, *7*, 5497. doi:10.1021/OL0522891

[15] N. Sayyadi, *Ph.D. Thesis: Pseudoprolines: A Versatile New Tool for the Synthesis of Cyclic Peptides*, University of Sydney, **2008**.

[16] K. Wüthrich, *NMR of Proteins and Nucleic Acids* **1986**, p. 117 (John Wiley & Sons, Inc.: New York, NY).

[17] D. Pal, P. Chakrabarti, *J. Mol. Biol.* **1999**, *294*, 271. doi:10.1006/JMBI.1999.3217
[18] A. Nefzi, K. Schenk, M. Mutter, *Protein Pept. Lett.* **1994**, *1*, 66.
[19] *SMART SAINT and XPREP, Bruker* **1995** (Bruker Analytical X-ray Instruments Inc.: Madison, WI).
[20] *teXsan for Windows: Single Crystal Structure Analysis Software* **1997–1998** (Molecular Structure Corporation: The Woodlands, TX).
[21] L. J. Farrugia, *J. Appl. Cryst.* **1999**, *32*, 837. doi:10.1107/S0021889899006020
[22] *Xtal3.6 System* (Eds S. R. Hall, D. J. du Boulay, R. Olthof-Hazekamp) **1999** (University of Western Australia).
[23] A. Altomare, M. C. Burla, M. Camalli, G. L. Cascarano, C. Giocavazzo, A. Guagliardi, A. G. C. Moliterni, G. Polidori, R. Spagna, *J. Appl. Cryst.* **1999**, *32*, 115. doi:10.1107/S0021889898007717
[24] G. M. Sheldrick, *SADABS: Empirical Absorption and Correction Software* **1999–2003** (University of Göttingen: Germany).
[25] P. Coppens, L. Leiserowitz, D. Rabinovich, *Acta Crystallogr.* **1965**, *18*, 1035. doi:10.1107/S0365110X65002487
[26] G. M. Sheldrick, *SHELXL-97: Programs for Crystal Structure Analysis* **1997** (University of Göttingen: Germany).